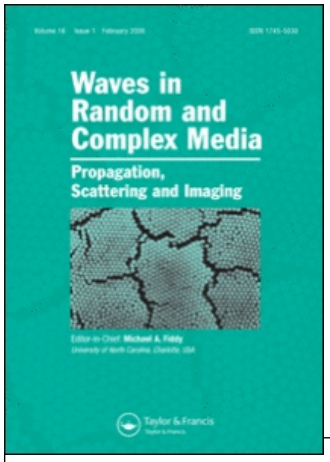

Waves in Random and Complex Media

Publication details, including instructions for authors and subscription information:
http://www.informaworld.com/smpp/title~content=t716100762

Scattering by an object above a randomly rough surface from a fast numerical method: Extended PILE method combined with FB-SA

G. Kubické [a]; C. Bourlier [a]; J. Saillard [a]

[a] La Chantrerie, IREENA, Ecole Polytechnique de l'Université de Nantes, Nantes, Cedex 3, France

Online Publication Date: 01 August 2008

To cite this Article: Kubické, G., Bourlier, C. and Saillard, J. (2008) 'Scattering by an object above a randomly rough surface from a fast numerical method: Extended PILE method combined with FB-SA', Waves in Random and Complex Media, 18:3, 495 — 519

To link to this article: DOI: 10.1080/17455030802087057
URL: http://dx.doi.org/10.1080/17455030802087057

Waves in Random and Complex Media
Vol. 18, No. 3, August 2008, 495–519

Scattering by an object above a randomly rough surface from a fast numerical method: Extended PILE method combined with FB-SA

G. Kubické*, C. Bourlier and J. Saillard

IREENA, Ecole Polytechnique de l'Université de Nantes, La Chantrerie, Nantes Cedex 3, France

(*Received 21 January 2008; final version received 26 March 2008*)

In this paper, a fast exact numerical method, based on the method of moments, is developed to calculate the scattering by an object above a rough surface. N. Déchamps et al. have recently developed the PILE (Propagation-Inside-Layer Expansion) method for a stack of two one-dimensional rough interfaces separating homogeneous media. This method allows us to calculate separately and exactly the multiple scattering contributions inside the layer. This is done with a decomposition by block of the impedance matrix (the inverse of the impedance matrix of each interface and two coupling matrices are involved). The purpose of this paper is to extend the PILE method to the more general case of two illuminated surfaces and to apply it to an object located above a rough surface. In addition, to invert a matrix of large size, the Forward–Backward Spectral Acceleration (FB-SA) approach of complexity $\mathcal{O}(N)$ proposed by Chou and Johnson is applied. The new method, extended PILE combined with FB-SA, is tested on Perfectly Conducting (PC) circular and elliptic cylinders located above a rough surface (dielectric or PC) obeying a Gaussian process with Gaussian and exponential height autocorrelation functions.

1. Introduction

The study of scattering by an object located in front of an interface is a subject of great interest. The origin of this question dates back to the problem studied by Sommerfeld [1] concerning a dipole in front of a conducting half-space.

In recent times there has been increasing interest in the scattering of an electromagnetic wave by a cylinder or sphere near a smooth surface [2–6]. Many areas are concerned by these works, such as the study of surfaces of contaminated particles for example. Moreover, in the more general case of an object located above a rough surface, other applications are concerned, such as remote sensing, radar surveillance, and so on. In this configuration, some asymptotic models and exact numerical methods have been investigated [7–13].

But, in the numerical simulations of the scattering by an object above a rough surface, the length of the surface plays an important role: it has to be large enough for the scattered field to vanish at the surface extremities, that is, to avoid edge effect. Thus, it is interesting to investigate exact fast numerical methods to treat a large problem. Such methods have been developed for a single rough surface. For instance, one can quote the Banded-Matrix-Iterative-Approach/CAnonical Grid (BMIA-CAG) of Tsang et al. [14, 15] of complexity $\mathcal{O}(N \log N)$, the Forward–Backward (FB) method of Holliday et al. [16] of complexity $\mathcal{O}(N^2)$, and the accelerated version Forward–Backward Spectral Acceleration (FB-SA) of Chou et al. [17, 18] of complexity

*Corresponding author. Email: gildas.kubicke@univ-nantes.fr

ISSN: 1745-5030 print / 1745-5049 online

DOI: 10.1080/17455030802087057
http://www.informaworld.com

$\mathcal{O}(N)$, in which N is the number of samples on the surface. Pino et al. [7] studied scattering by an object located *on* a rough surface. In this study, the object surface is included in the surface contour of the rough surface. The Forward–Backward method was generalized to this problem and then the Spectral Acceleration was applied in [19]. For the problem of an object located *above* a rough surface, this method cannot be applied since there are two different and distinct surfaces.

Recently, N. Déchamps et al. [20] have developed a fast numerical method, PILE (Propagation-Inside-Layer Expansion), devoted to the scattering by a stack of two one-dimensional interfaces separating homogeneous media. More recently, C. Bourlier et al. [21] have applied the PILE method for an object located below a rough surface. In these articles, only the upper surface was illuminated. The main advantage of the PILE method is that the resolution of the linear system (obtained from the method of moments) is broken up into different steps:

(i) Two steps are dedicated to solving for the local interactions, which can be done from efficient methods valid for a single rough interface, such FB-SA and BMIA/CAG.
(ii) Two are dedicated to solving for the coupling interactions, which can be done by updating the previous efficient methods. This has been recently investigated with BMIA/CAG [22] and FB-SA [23].

The purpose of this paper is to extend the PILE method to the more general case of two illuminated surfaces and to apply this extended PILE method to an object located above a rough surface. In addition to accelerate the extended PILE and to treat a large problem, the local interactions on the lower surface are computed from FB-SA. Since the unknown number on the surface is much greater than that on the object, the method complexity is then $\mathcal{O}(N)$.

This paper is organized as follows. In Section 2, the geometry of the problem is defined. In Section 3, the extended PILE method is investigated and its convergence is studied for perfectly conducting circular and elliptic cylinders located above a rough surface. In Section 4, the extended PILE method combined with FB-SA for the calculation of the local interactions on the lower rough interface is presented and its convergence is investigated.

2. Geometry of the problem

Let us assume that the object and the rough surface are invariant along the $\hat{\mathbf{y}}$ direction and that the incident wavevector is lying in the $(\hat{\mathbf{x}}, \hat{\mathbf{z}})$ plane. Consequently, the problem is two-dimensional. As a result, the object and the surface are defined by one-dimensional surfaces: Σ_+ and Σ_- of equation z_+ and z_-, respectively. The scene is depicted in Figure 1. The height z_- is assumed to be a Gaussian stationary stochastic process with zero mean value ($\langle z_- \rangle = 0$). The surface height spectrum can be of any kind. The height z_+ is a deterministic function defined with respect to its centre $\{x_c, h_c\}$ with $h_c > 0$ (height). Care must be taken to avoid any intersection between z_+ and z_-. By using a spectral method, widely used in the calculation of wave scattering [24], the random surface Σ_- can easily be generated. The discretized abscissa and heights of the rough surface are given by $x_-^n = -\frac{L_-}{2} + (n - \frac{1}{2})\Delta x_-$ and $z_-^n = z_-(x_-^n)$, respectively, with $n \in [1; N_-]$, where N_- represents the number of samples. $\Delta x_- = L_-/N_-$ is the sampling step and L_- the length of the surface. In the same manner, one defines for the object $z_+^m = z_+(x_+^m)$ with $m \in [1; N_+]$, where N_+ is the number of samples. According to the object shape, z_+ must be a bijective function. For example for an elliptic cylinder of major and minor semi-axis $\{a, b\}$, the polar coordinates ($a, b, \phi \in [0; 2\pi]$) are used to express a point location on the cylinder. This leads to $\{x_+ = x_c + a\cos\phi, z_+ = h_c + b\sin\phi\}$. For a circular cylinder $a = b$, where a is

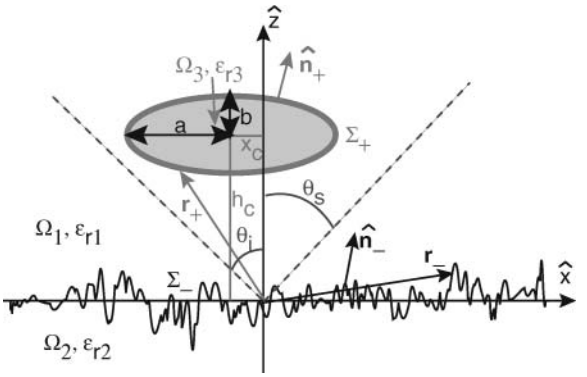

Figure 1. Geometry of the problem.

the radius. A point of the plane $(\hat{\mathbf{x}}, \hat{\mathbf{z}})$ will be denoted by $\mathbf{r} = x\hat{\mathbf{x}} + z\hat{\mathbf{z}}$ and a point belonging to $\Sigma_\pm$ by $\mathbf{r}_\pm = x_\pm\hat{\mathbf{x}} + z_\pm\hat{\mathbf{z}}$. The random interface is separated by two non-magnetic semi-infinite homogeneous media $\Omega_{1,2}$ of relative permittivity $\epsilon_{r1,r2}$, and the relative permittivity of the non-magnetic object is ϵ_{r3}.

To avoid edge limitations, the incident field ψ_i is chosen as a Thorsos tapered plane wave [25] defined as

$$\psi_i(\mathbf{r}) = \exp(j\mathbf{k}_i \cdot \mathbf{r}) \exp\left(-\frac{(x + z\tan\theta_i)^2}{g^2} \right) \exp[jw(\mathbf{r})\mathbf{k}_i \cdot \mathbf{r}], \tag{1}$$

in which $w(\mathbf{r}) = [\frac{2(x+z\tan\theta_i)^2}{g^2} - 1]/(K_1 g\cos\theta_i)^2$ and $\mathbf{k}_i = K_1(\hat{\mathbf{x}}\sin\theta_i - \hat{\mathbf{z}}\cos\theta_i)$ is the incident wavevector. θ_i is the incident angle defined with respect to $\hat{\mathbf{z}}$ in the counterclockwise direction (Figure 1), K_1 is the wavenumber in the incident medium Ω_1, g stands for the tapering parameter which has a dimension of length (controls the spatial extent of the incident wave). Since the paper is devoted to moderate incidence angles, this wave is appropriate and satisfies Maxwell's equations with good accuracy. An $e^{-j\omega t}$ time-harmonic convention is used. Furthermore, the TE (electric field along the $\hat{\mathbf{y}}$ direction) and TM (magnetic field along the $\hat{\mathbf{y}}$ direction) polarizations are considered.

3. The extended PILE (Propagation-Inside-Layer-Expansion) method

3.1. *Mathematical formulation*

Déchamps et al. [20] have developed a new method to reduce complexity of the study of electromagnetic scattering from a stack of two one-dimensional rough interfaces separating homogeneous media. For this case, only the upper surface was excited by the incident field. In this paper, the PILE method must be updated since the object and the rough surface are both excited by the incident field. Consequently, the extended PILE method proposed in this paper is a generalization of the PILE method, for the case of scattering by two illuminated surfaces. The main equations are given hereafter. Using the extinction theorem both on the rough interface and object and the boundary conditions, we obtain four coupled integral equations (see for instance [9,20,26]).

The use of the method of moments with point matching and pulse basis functions leads to the following linear system

$$\bar{\mathbf{Z}}\mathbf{X} = \mathbf{s}, \tag{2}$$

where $\bar{\mathbf{Z}}$ (the over-bar stands for a matrix) is the impedance matrix of size $2(N_+ + N_-) \times 2(N_+ + N_-)$. The unknown vector $\mathbf{X}$ of length $2(N_+ + N_-)$ is equal to

$$\mathbf{X}^T = [\mathbf{X}_+^{\mathrm{T}} \mathbf{X}_-^{\mathrm{T}}], \tag{3}$$

where ^{T} stands for the transpose operator. $\mathbf{X}_\pm$ of length $2N_\pm$ contains the unknown fields $\psi_\pm$ and their normal derivatives $\partial\psi_\pm/\partial n_\pm$ on the object and on the lower surface

$$\mathbf{X}_\pm^T = \left[\underbrace{\psi(r_\pm^1) \ \ldots \ \psi(r_\pm^{N_\pm})}_{N_\pm \text{ times}} \ \underbrace{\frac{\partial\psi(r_\pm^1)}{\partial n_\pm} \ \ldots \ \frac{\partial\psi(r_\pm^{N_\pm})}{\partial n_\pm}}_{N_\pm \text{ times}} \right]. \tag{4}$$

The source term $\mathbf{s}$ is defined as

$$\mathbf{s}^{\mathrm{T}} = [\mathbf{s}_+^{\mathrm{T}} \mathbf{s}_-^{\mathrm{T}}], \tag{5}$$

with

$$\mathbf{s}_\pm^{\mathrm{T}} = \left[\underbrace{\psi_i(r_\pm^1) \ \ldots \ \psi_i(r_\pm^{N^\pm})}_{N_\pm \text{ times}} \ \underbrace{0 \ \ldots \ 0}_{N_\pm \text{ times}} \right]. \tag{6}$$

To solve efficiently the linear system (2), the impedance matrix $\bar{\mathbf{Z}}$ is expressed from submatrices [20] as

$$\bar{\mathbf{Z}} = \begin{bmatrix} \bar{\mathbf{Z}}_+ & \bar{\mathbf{Z}}_\mp \\ \bar{\mathbf{Z}}_\pm & \bar{\mathbf{Z}}_-. \end{bmatrix}. \tag{7}$$

$\{\bar{\mathbf{Z}}_+, \bar{\mathbf{Z}}_-\}$ correspond exactly to the impedance matrices (size $(2N_\pm) \times (2N_\pm)$) of $\Sigma_\pm$. The matrices $\bar{\mathbf{Z}}_\mp$ (size $(2N_-) \times (2N_+)$) and $\bar{\mathbf{Z}}_\pm$ (size $(2N_+) \times (2N_-)$) can be interpreted as coupling matrices between Σ_+ and Σ_-. Complete expressions for these matrices can be found in Appendix A. In contrast to the case of a stack of two rough interfaces [20] ($\mathbf{s}_+ \neq \mathbf{0}$, $\mathbf{s}_- = \mathbf{0}$), the two surfaces are illuminated by the incident field ($\mathbf{s}_+ \neq \mathbf{0}$, $\mathbf{s}_- \neq \mathbf{0}$). The extended PILE method proposed in this paper is then generalized in order to introduce the fact that $\mathbf{s}_- \neq \mathbf{0}$. From [27] we have

$$\bar{\mathbf{Z}}^{-1} = \begin{bmatrix} \bar{\mathbf{T}} & \bar{\mathbf{U}} \\ \bar{\mathbf{V}} & \bar{\mathbf{W}} \end{bmatrix}, \tag{8}$$

with

$$\begin{cases} \bar{\mathbf{T}} = (\bar{\mathbf{Z}}_+ - \bar{\mathbf{Z}}_\mp \bar{\mathbf{Z}}_-^{-1} \bar{\mathbf{Z}}_\pm)^{-1} \\ \bar{\mathbf{U}} = -(\bar{\mathbf{Z}}_+ - \bar{\mathbf{Z}}_\mp \bar{\mathbf{Z}}_-^{-1} \bar{\mathbf{Z}}_\pm)^{-1} \bar{\mathbf{Z}}_\mp \bar{\mathbf{Z}}_-^{-1} \\ \bar{\mathbf{V}} = -\bar{\mathbf{Z}}_-^{-1} \bar{\mathbf{Z}}_\pm (\bar{\mathbf{Z}}_+ - \bar{\mathbf{Z}}_\mp \bar{\mathbf{Z}}_-^{-1} \bar{\mathbf{Z}}_\pm)^{-1} \\ \bar{\mathbf{W}} = \bar{\mathbf{Z}}_-^{-1} + \bar{\mathbf{Z}}_-^{-1} \bar{\mathbf{Z}}_\pm (\bar{\mathbf{Z}}_+ - \bar{\mathbf{Z}}_\mp \bar{\mathbf{Z}}_-^{-1} \bar{\mathbf{Z}}_\pm)^{-1} \bar{\mathbf{Z}}_\mp \bar{\mathbf{Z}}_-^{-1} \end{cases} \tag{9}$$

and the unknown vector $\mathbf{X}$ is obtained as:

$$\begin{bmatrix} \mathbf{X}_+ \\ \mathbf{X}_- \end{bmatrix} = \bar{\mathbf{Z}}^{-1} \begin{bmatrix} \mathbf{s}_+ \\ \mathbf{s}_- \end{bmatrix} = \begin{bmatrix} \bar{\mathbf{T}} \cdot \mathbf{s}_+ + \bar{\mathbf{U}} \cdot \mathbf{s}_- \\ \bar{\mathbf{V}} \cdot \mathbf{s}_+ + \bar{\mathbf{W}} \cdot \mathbf{s}_- \end{bmatrix}. \tag{10}$$

By using Equations (9) and (10), the total field on the object $\mathbf{X}_+$ can be expressed as

$$\mathbf{X}_+ = (\bar{\mathbf{Z}}_+ - \bar{\mathbf{Z}}_\mp \bar{\mathbf{Z}}_-^{-1} \bar{\mathbf{Z}}_\pm)^{-1} \mathbf{s}_+ - (\bar{\mathbf{Z}}_+ - \bar{\mathbf{Z}}_\mp \bar{\mathbf{Z}}_-^{-1} \bar{\mathbf{Z}}_\pm)^{-1} \bar{\mathbf{Z}}_\mp \bar{\mathbf{Z}}_-^{-1} \mathbf{s}_-, \tag{11}$$

which leads to

$$\begin{aligned} \mathbf{X}_+ &= (\bar{\mathbf{Z}}_+ - \bar{\mathbf{Z}}_\mp \bar{\mathbf{Z}}_-^{-1} \bar{\mathbf{Z}}_\pm)^{-1} (\mathbf{s}_+ - \bar{\mathbf{Z}}_\mp \bar{\mathbf{Z}}_-^{-1} \mathbf{s}_-) \\ &= (\bar{\mathbf{I}} - \bar{\mathbf{Z}}_+^{-1} \bar{\mathbf{Z}}_\mp \bar{\mathbf{Z}}_-^{-1} \bar{\mathbf{Z}}_\pm)^{-1} \bar{\mathbf{Z}}_+^{-1} (\mathbf{s}_+ - \bar{\mathbf{Z}}_\mp \bar{\mathbf{Z}}_-^{-1} \mathbf{s}_-), \end{aligned} \tag{12}$$

where $\bar{\mathbf{I}}$ is the identity matrix. Let us introduce the characteristic matrix $\bar{\mathbf{M}}_{c,+}$ as

$$\bar{\mathbf{M}}_{c,+} = \bar{\mathbf{Z}}_+^{-1} \bar{\mathbf{Z}}_\mp \bar{\mathbf{Z}}_-^{-1} \bar{\mathbf{Z}}_\pm. \tag{13}$$

The first term in Equation (12) can be expanded as an infinite series over p

$$\left(\bar{\mathbf{I}} - \bar{\mathbf{Z}}_+^{-1} \bar{\mathbf{Z}}_\mp \bar{\mathbf{Z}}_-^{-1} \bar{\mathbf{Z}}_\pm\right)^{-1} = \sum_{p=0}^{p=\infty} \bar{\mathbf{M}}_{c,+}^p. \tag{14}$$

For the numerical computation, the sum must be truncated at order P_{PILE}. From Equations (12) and (14), the total field on the object $\mathbf{X}_+$ is then expressed as

$$\mathbf{X}_+ = \left[\sum_{p=0}^{p=P_{\text{PILE}}} \bar{\mathbf{M}}_{c,+}^p \right] \bar{\mathbf{Z}}_+^{-1} (s_+ - \bar{\mathbf{Z}}_\mp \bar{\mathbf{Z}}_-^{-1} \mathbf{s}_-) = \sum_{p=0}^{p=P_{\text{PILE}}} \mathbf{Y}_+^{(p)}, \tag{15}$$

in which

$$\begin{cases} \mathbf{Y}_+^{(0)} = \bar{\mathbf{Z}}_+^{-1} (\mathbf{s}_+ - \bar{\mathbf{Z}}_\mp \bar{\mathbf{Z}}_-^{-1} \mathbf{s}_-) & \text{for } p = 0 \\ \mathbf{Y}_+^{(p)} = \bar{\mathbf{M}}_{c,+} \mathbf{Y}_+^{(p-1)} & \text{for } p > 0 \end{cases}. \tag{16}$$

The unknown vector $\mathbf{X}_-$ is obtained by substituting in Equations (15), (16) and (13), subscripts $\{+, -, \pm, \mp\}$ for subscripts $\{-, +, \mp, \pm\}$, respectively.

We define the norm $|\bar{\mathbf{M}}_{c,+}|$ of a complex matrix by its spectral radius, i.e. the modulus of its eigenvalue which has the highest modulus. Expansion (14) is then valid if $|\bar{\mathbf{M}}_{c,+}|$ is strictly smaller than one. The physical interpretation of $\bar{\mathbf{M}}_{c,+}$ is shown in Figure 2: in the zeroth order term, $\bar{\mathbf{Z}}_+^{-1}$ accounts for the local interactions on the upper surface, so $\mathbf{Y}_+^{(0)}$ corresponds to the contribution of the scattering on the object when it is illuminated by the direct incident field ($\mathbf{s}_+$) and the direct scattered field by the lower surface ($-\bar{\mathbf{Z}}_\mp \bar{\mathbf{Z}}_-^{-1} \mathbf{s}_-$). Indeed, $\bar{\mathbf{Z}}_-^{-1}$ accounts for the local interactions on the lower surface, and $\bar{\mathbf{Z}}_\mp$ propagates the field on the lower surface toward the object. In the first order term, $\mathbf{Y}_+^{(1)} = \bar{\mathbf{M}}_{c,+} \mathbf{Y}_+^{(0)}$, $\bar{\mathbf{Z}}_\pm$ propagates the resulting upper

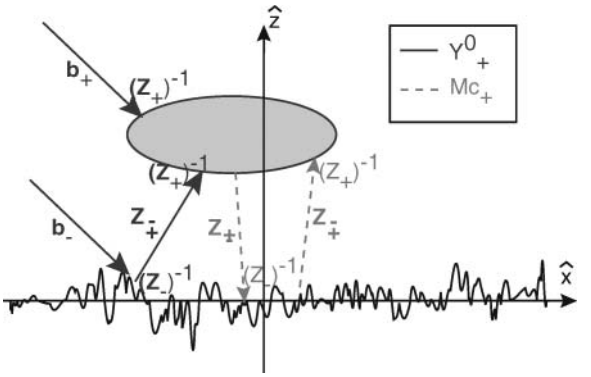

Figure 2. Illustration of the physical interpretation of the extended PILE method.

field information, $\mathbf{Y}_+^{(0)}$, toward the lower surface (the rough surface), $\bar{\mathbf{Z}}_-^{-1}$ accounts for the local interactions on this surface, and $\bar{\mathbf{Z}}_{\mp}$ re-propagates the resulting contribution toward the upper surface (the object); finally, $\bar{\mathbf{Z}}_+^{-1}$ updates the field values on the object. So the characteristic matrix $\bar{\mathbf{M}}_{c,+}$ realizes a back and forth between the upper surface and the lower one. In conclusion, the order P_{PILE} of PILE, corresponds to the P_{PILE} back and forth between the surface and the object. In the same manner, $\bar{\mathbf{M}}_{c,-}$ realizes a back and forth between the lower surface and the object.

3.2. *Convergence of PILE*

The purpose of this subsection is to study the convergence of PILE versus its order, P_{PILE}. In what follows, the abscissa of the object is $x_c = 0$, a will denote the radius of a circular cylinder and h_c its height. To study the convergence, a criterion is introduced by using the Relative Residual Error (RRE) defined as

$$\text{RRE} : r_e = \frac{\text{norm}\,(\mathbf{X} - \mathbf{X}_{\text{LU}})}{\text{norm}\,(\mathbf{X}_{\text{LU}})}. \tag{17}$$

The norm of a vector of components X_i and of length N is expressed as $\text{norm}(\mathbf{X}) = \sum_{i=1}^{i=N} |X_i|^2$. $\mathbf{X}$ represents either the field ψ or its normal derivative $\partial\psi/\partial n$ on the surface. The subscript LU means that the vector is computed from a LU inversion (benchmark solution). So, for a low RRE, the vector $\mathbf{X}$ obtained from the extended PILE method is close to $\mathbf{X}_{\text{LU}}$ computed from the benchmark method: the direct LU inversion. In what follows, the surface is assumed to be a Gaussian process with a Gaussian height spectrum and the incident medium Ω_1 is the vacuum (the incident wavelength is denoted as λ_0).

In Figure 3, the scattering coefficient in the dB scale is compared with that obtained from a direct LU inversion versus the scattering angle θ_s and for different orders P_{PILE}. From a Thorsos wave and for $\mathbf{r} \in \Omega_1$, it is equal to [24]

$$\sigma_s(\theta_i, \theta_s) = \frac{\left|\psi_{s_+}^{\infty} + \psi_{s_-}^{\infty}\right|^2}{8\pi K_0 g \cos\theta_i \left[1 - \frac{1+2\tan^2\theta_i}{2K_0^2 g^2 \cos^2\theta_i}\right]}, \tag{18}$$

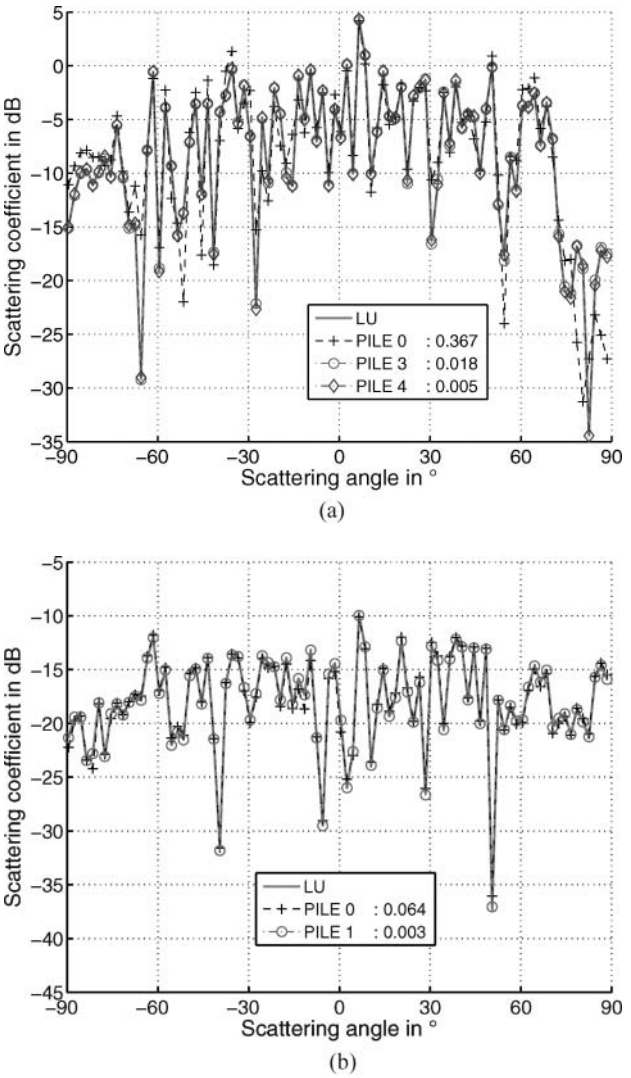

Figure 3. Comparison of the scattering coefficient in the dB scale with the one obtained from a direct LU inversion versus the scattering angle θ_s. $\theta_i = 0^\circ$, $L_c = 2\lambda_0$, $\sigma_z = \lambda_0$, $N_- = 1200$, $L_- = 120\lambda_0$, $g = L_-/6$, $N_+ = 63$, $h_c = 4\lambda_0$ and $a = 1\lambda_0$. In each subfigure, the order of PILE and the corresponding RRE (largest value of the RRE computed over the field and its normal derivative for both surfaces) are mentioned in the legend. At the top, PC rough surface case ($\epsilon_{r2} = j\infty$), and at the bottom dielectric rough surface case ($\epsilon_{r2} = 2 + 0.01j$).

with

$$\psi_{s_p}^{\infty} = + \int_{\Sigma_p} \left\{ jK_0\psi_p[\gamma_p \sin\theta_s - \cos\theta_s] - \frac{\partial\psi_p}{\partial n_p}\sqrt{1+\gamma_p^2} \right\} e^{-j\mathbf{k}_s\cdot\mathbf{r}} dx_p, \tag{19}$$

where p equals $+$ or $-$, $\mathbf{k}_s = K_0(\hat{\mathbf{x}}\sin\theta_s + \hat{\mathbf{z}}\cos\theta_s)$ ($K_0 = 2\pi/\lambda_0$) the scattering wavevector and $\gamma_p = \partial z_p/\partial x_p$. Care must be taken in Equation (19): the normal of the object must be oriented toward the outside of the object (this comment also holds for the impedance matrix calculation,

Table 1. Order P_{PILE} versus σ_z/λ_0 for a circular cylinder above a rough surface and for the TE and TM polarizations. Five cases are considered. Correlation length $L_c = 2\lambda_0$, sampling step $\lambda_0/10$ for the rough surface of length $L_- = 120\lambda_0$ ($N_- = 1200$), Thorsos wave parameter $g = L_-/6$, $N_+ = 63$, $h_c = 4\lambda_0$ and $a = 1\lambda_0$.

σ_z/λ_0 θ_i in$^\circ$, ϵ_{r2}	0.5 TE-TM	1 TE-TM	1.5 TE-TM	2 TE-TM
(a): 0, $j\infty$ (PC)	2−2	4−4	5−5	5−4
(b): 60, $j\infty$ (PC)	2−2	3−3	5−3	4−3
(c): 0, $2 + 0.01j$	1−1	1−1	1−1	1−1
(d): 60, $2 + 0.01j$	1−1	1−1	1−1	1−2
(e): 0, $10 + j$	2−2	2−2	3−2	2−2

see Appendix A for more details). The parameters are $\theta_i = 0^\circ$, $L_c = 2\lambda_0$, $\sigma_z = \lambda_0$, $N_- = 1200$, $L_- = 120\lambda_0$, $g = L_-/6$, $N_+ = 63$, $h_c = 4\lambda_0$ and $a = 1\lambda_0$ and for TE polarization. In addition, the scattering coefficient obtained from a direct LU inversion is plotted. Since the RRE decreases when the order P_{PILE} increases, one can conclude that good convergence is obtained.

Figure 4 presents, for different orders P_{PILE}, the modulus of the total radiated field, $\psi_{\text{rad}}(\mathbf{r})$, computed from the fields on the rough surface and the object versus the normalized abscissa x/λ_0 and the normalized height h/λ_0 for the TE polarization. It is expressed as

$$\psi_{\text{rad}}(\mathbf{r}) = s'\psi_i(\mathbf{r}) + \sum_{p=\pm} s_p \int_{\Sigma_p} \left(\psi_p(\mathbf{r}_p) \frac{\partial g_p(\mathbf{r}_p, \mathbf{r})}{\partial n_p} - g_p(r_p, r) \frac{\partial \psi_p(\mathbf{r}_p)}{\partial n_p} \right) d\Sigma_p, \tag{20}$$

with $\mathbf{r} \notin (\Sigma_+ \cup \Sigma_-)$ (and Ω_3 if the object is a perfect conductor), $\{s_\pm = +1, s' = +1\}$ if $\mathbf{r} \in \Omega_1$ else $\{s_+ = 0, s_- = -1, s' = 0\}$, $g_p(\mathbf{r}_p, \mathbf{r}) = \frac{j}{4} H_0^{(1)}(K_0 \sqrt{\epsilon_{rp}} \|\mathbf{r}_p - \mathbf{r}\|)$, in which $\epsilon_{rp} = \epsilon_{ri}$ if $\mathbf{r} \in \Omega_i$. The parameters are the same as in Figure 3(b), but $\sigma_z = 0.5\lambda_0$, $L_- = 80\lambda_0$, $\theta_i = 20^\circ$ and $g = L_-/4$. Figure 4 clearly shows that the PILE order is related to the number of reflections between the surface and the cylinder.

In order to obtain the order P_{PILE} which permits us to provide good convergence, the Relative Residual Error (RRE) must be smaller than a threshold chosen equal to 10^{-2} in what follows. So, the order P_{PILE} is obtained when r_e becomes smaller than 10^{-2}. Since r_e is determined for ψ and $\partial\psi/\partial n$, we take the largest value of P_{PILE}.

Table 1 presents the order P_{PILE} for a circular cylinder above a rough surface (PC or dielectric) and for the TE and TM polarizations. It is computed from one surface realization. The parameters are $L_c = 2\lambda_0$, $\sigma_z \in [0.5; 2]\lambda_0$, sampling step $\lambda_0/10$ for the rough surface of length $L_- = 120\lambda_0$ ($N_- = 1200$), Thorsos wave parameter $g = L_-/6$, $N_+ = 63$, $h_c = 4\lambda_0$ and $a = 1\lambda_0$. Five cases are considered. Moreover, the energy conservation is given for the PC rough surface cases in Table 2.

Table 2. Energy conservation versus σ_z/λ_0 for a circular cylinder above a rough PC surface and for the TE and TM polarizations. The parameters are the same as in Table 1 but only cases (a) and (b) are considered.

σ_z/λ_0 θ_i in$^\circ$, ϵ_{r2}	0.5 TE−TM	1 TE−TM	1.5 TE−TM	2 TE−TM
(a): 0, $j\infty$ (PC)	1.000−0.991	0.998−1.010	0.990−1.061	1.000−1.006
(b): 60, $j\infty$ (PC)	0.990−0.994	0.996−1.007	0.997−1.026	0.997−1.032

Table 3. Order P_{PILE} versus a/λ_0 for an elliptic cylinder above a rough PC surface and for the TE and TM polarizations. The parameters are $L_c = 2\lambda_0$, $\sigma_z = 0.5\lambda_0$, sampling step $\lambda_0/10$ for the rough surface of length $L_- = 120\lambda_0$ ($N_- = 1200$), $\theta_i = 0^\circ$, $g = L_-/6$, $h_c = 4\lambda_0$, $b = \lambda_0$ (semi-minor axis and $a \geq b$).

a/λ_0	1 $N_+ = 63$	2 $N_+ = 97$	3 $N_+ = 134$	4 $N_+ = 172$	5 $N_+ = 210$
TE	2	12	43	66	46
TM	2	12	39	56	40

As the modulus of the permittivity, $|\epsilon_{r2}|$, increases, the order P_{PILE} increases. Indeed, the reflection by the surface is strong with a high value $|\epsilon_{r2}|$, that increases the energy reflected toward the cylinder. This implies that the number of reflections between the rough surface and the object contributing to the scattering process increases. Table 1 reveals also that P_{PILE} is quasi-independent of the incidence angle θ_i and the polarization. The energy conservation, which is a good criterion to test the validity of the approach, is equal to $1 \pm 1\%$ except for three cases. In TM polarization, for $\sigma_z/\lambda_0 = 1.5$, $\theta_i = 0^\circ$, for $\sigma_z/\lambda_0 = 1.5$, $\theta_i = 60^\circ$ and for $\sigma_z/\lambda_0 = 2$, $\theta_i = 60^\circ$, the energy conservation is not satisfied. This fact is also observed for the case without object. Indeed, when σ_z is high, the field on the rough surface does not vanish on the edges. In fact, the integral equations cannot be applied if the field does not vanish on the edge of the surface. It is important to notice that this is not due to the use of the PILE method since this phenomenon is also observed with the direct LU inversion. A solution could be to take a higher surface length, which implies the need to investigate exact fast numerical methods to treat a large problem.

Tables 3 and 4 present, respectively, the order P_{PILE} and the energy conservation, for an elliptic cylinder above a PC rough surface and for the TE and TM polarizations. The parameters are $L_c = 2\lambda_0$, $\sigma_z = 0.5\lambda_0$, sampling step $\lambda_0/10$ for the rough surface of length $L_- = 120\lambda_0$ ($N_- = 1200$), $\theta_i = 0^\circ$, $g = L_-/6$, $h_c = 4\lambda_0$, $b = \lambda_0$ (semi-minor axis and $a \geq b$).

As the semi-major axis a increases, the order P_{PILE} increases, which means that the interactions between the object and the rough surface are stronger. Indeed, as the elliptic cylinder is more elongated, the region located between the object and the lower surface is comparable to an open wave guide. The wave is guided between the two surfaces, which induces a lot of reflections and so, a high order P_{PILE}. For $a/\lambda_0 = 3$ in TM polarization, the energy conservation is not satisfied. In this case, the field on the rough surface does not vanish on the edges. This is due to the elliptic cylinder which provides a diffracted field on the surface far away from the origin. This field contribution attenuates in free space slower in TM polarization than in TE polarization. As seen before, a solution could be to take a higher surface length.

If the object dimension is of the order of the wavelength and if Δx_- is of the order of Δx_+, then the number of samples on the surface Σ_- is much greater than that of the object Σ_+,

Table 4. Energy conservation versus a/λ_0 for an elliptic cylinder above a rough PC surface and for the TE and TM polarizations. The parameters are the same as in Table 3.

a/λ_0	1 $N_+ = 63$	2 $N_+ = 97$	3 $N_+ = 134$	4 $N_+ = 172$	5 $N_+ = 210$
TE	1.000	0.994	1.000	0.997	0.999
TM	0.991	0.994	1.040	0.993	1.001

$N_- \gg N_+$. Thus, the most complex operation in the calculation of $\mathbf{X}_+$ and $\mathbf{X}_-$ is $\bar{\mathbf{Z}}_-^{-1}\mathbf{u}$, where $\mathbf{u}$ is a vector. This calculation, which only concerns the local interactions on the lower surface, can be computed by fast numerical methods that already exist for a single rough surface. So, the next section explains how to proceed to speed up the matrix-vector product $\bar{\mathbf{Z}}_-^{-1}\mathbf{u}$ in the extended PILE method by using the Forward–Backward Spectral Acceleration.

4. Extended PILE method combined with the Forward–Backward Spectral Acceleration

Several methods can be used to speed up the matrix-vector product $\bar{\mathbf{Z}}_-^{-1}\mathbf{u}$, like for instance the Banded-Matrix-Iterative-Approach/CAnonical Grid (BMIA-CAG) of Tsang et al. [14, 15] of complexity $\mathcal{O}(N_- \log N_-)$, the Forward–Backward (FB) method of Holliday et al. [16] of complexity $\mathcal{O}(N_-^2)$, and the accelerated version Forward–Backward Spectral Acceleration (FB-SA) of Chou et al. [17, 18] of complexity $\mathcal{O}(N_-)$, what makes it the most attractive. This section will summarize the FB method and its accelerated version. A more detailed theory can be found in [17, 18, 21, 23].

4.1. *FB (Forward–Backward) method*

First, the FB method is applied to speed up the calculation of $\bar{\mathbf{Z}}_-^{-1}\mathbf{u}$ ($\mathbf{u}$ is the column vector of length $2N_-$) in order to reduce the complexity to $\mathcal{O}(N_-^2)$ instead of $\mathcal{O}(N_-^3)$ from a direct LU inversion. This method was developed by Holliday et al. [16] for a perfectly-conducting surface. More recently, Iodice has extended the method to a dielectric surface [28].

In the FB approach, the unknown vector $\mathbf{X}$ is split into forward and backward contributions. By assuming that the incident beam propagates from left to right, at any given surface point, the forward contribution $\mathbf{X}^f$ is due to the incident field and to the radiation of the surface points on the left of the current point. And the backward contribution $\mathbf{X}^b$ is due to the radiation of the surface points on the right of the current point. The equations governing the forward and backward components are then obtained, and an iterative procedure is applied. This iterative computation of the matrix-vector product $\bar{\mathbf{Z}}_-^{-1}\mathbf{u}$, permits us to reduce the complexity to $\mathcal{O}(N_-^2)$. Nevertheless, the convergence of this method depends on the choice of the order P_{FB} which is involved in the FB iterative scheme. More details can be found in [16, 21, 23, 28].

The parameter P_{FB} is obtained by studying the scattering from a single rough dielectric surface (without the object).

As for the study of the convergence of the extended PILE method (see Section 3.2), the order P_{FB} is obtained when the Relative Residual Error (RRE) is smaller than a threshold chosen equal to 10^{-2}. The RRE is given in Equation (17) in which $\mathbf{X}$ represents either the field or its normal derivative, on the surface Σ_-. Since r_e is determined for ψ_-, and $\partial\psi_-/\partial n_-$, we take the largest value of P_{FB}.

Table 5 presents the order P_{FB} for a single rough surface (PC or dielectric) and for the TE and TM polarizations. It is computed from one surface realization. The correlation length is $L_c = 2\lambda_0$, the RMS heights are $\sigma_z \in [0.1; 2]\lambda_0$ (RMS slope $\sigma_\gamma = \sqrt{2}\sigma_z/L_c \in [0.0707; 1.4142]$). The sampling step is $\lambda_0/10$, the surface length $L_- = 120\lambda_0$ ($N_- = 1200$) and Thorsos wave parameter $g = L_-/6$.

First, we can notice that the FB method converges very rapidly for a PC rough surface in TM polarization. The order P_{FB} seems to be few sensitive to the RMS height and the incidence angle. In addition, as $|\epsilon_{r2}|$ increases (except for $j\infty$), the order FB increases for the TE polarization, whereas it remains unchanged for the TM polarization.

Table 5. Order P_{FB} versus σ_z/λ_0 for a single rough surface (without object) and for the TE and TM polarizations. Three cases are considered. Correlation length $L_c = 2\lambda_0$, sampling step $\lambda_0/10$, surface length $L_- = 120\lambda_0$ ($N_- = 1200$) and Thorsos wave parameter $g = L_-/6$.

σ_z/λ_0 θ_i in°, ϵ_{r2}	0.1 TE−TM	0.5 TE−TM	1 TE−TM	1.5 TE−TM	2 TE−TM
(a): 0, $j\infty$ (PC)	5−1	5−1	6−2	6−2	7−3
(b): 60, $j\infty$ (PC)	6−1	6−1	6−2	6−2	6−2
(c): 0, $2 + 0.01j$	5−4	5−4	5−5	5−5	6−6
(d): 60, $2 + 0.01j$	5−5	5−5	5−5	5−5	6−6
(e): 0, $10 + j$	8−5	8−5	8−5	10−5	10−5

In Figure 5, the scattering coefficient in the dB scale is compared with the one obtained from a direct LU inversion versus the scattering angle θ_s. From Thorsos wave and for $\mathbf{r} \in \Omega_1$, it is equal to [24]

$$\sigma_s(\theta_i, \theta_s) = \frac{\left|\psi_{s_-}^{\infty}\right|^2}{8\pi K_0 g \cos\theta_i \left[1 - \frac{1+2\tan^2\theta_i}{2K_0^2 g^2 \cos^2\theta_i}\right]}, \tag{21}$$

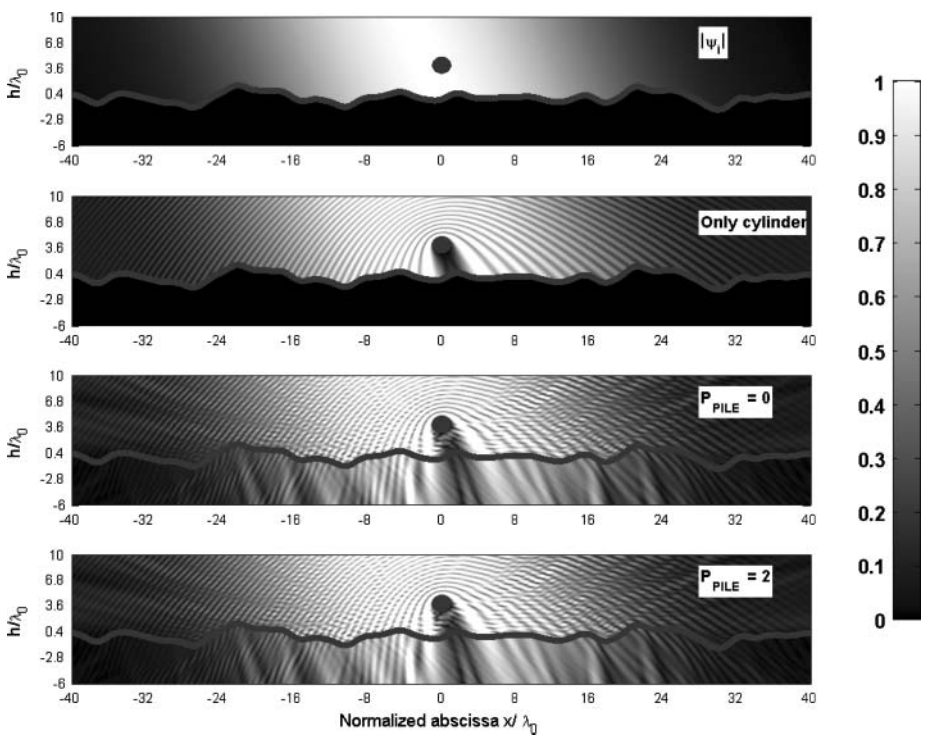

Figure 4. Modulus of the radiated field computed from the fields on the rough surface and the object versus the normalized abscissa x/λ_0 and the normalized height h/λ_0 for the TE polarization and for different orders P_{PILE}. The parameters are the same as in Figure 3(b), but $\sigma_z = 0.5\lambda_0$, $L_- = 80\lambda_0$, $\theta_i = 20°$ and $g = L_-/4$. In addition, the modulus of the radiated field computed from the fields on the cylinder, when it is considered alone, is plotted.

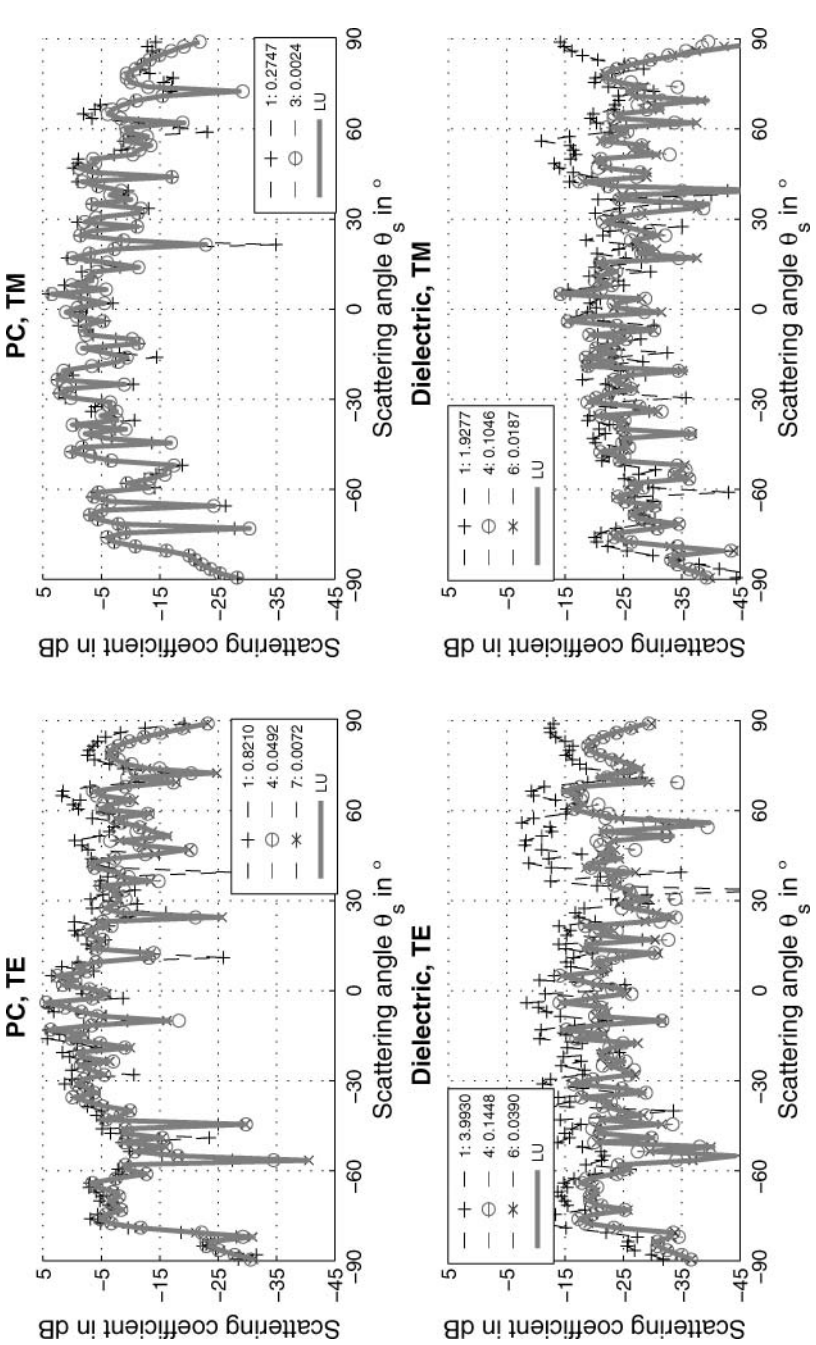

Figure 5. Comparison of the scattering coefficient (without object) in the dB scale with the one obtained from a direct LU inversion versus the scattering angle θ_s. At the top, PC case ($\epsilon_{r2} = j\infty$) and at the bottom, dielectric case ($\epsilon_{r2} = 2 + 0.01j$) for TE and TM polarizations. In the legend, the order P_{FB} and the RRE in a linear scale over the scattering coefficient are given. The parameters are the same as in Table 5 with $\theta_i = 0^\circ$ and $\sigma_z = 2\lambda_0$ ((a) and (c) cases).

with $\psi_{s_-}^{\infty}$ given by Equation (19). At the top, PC case and at the bottom, dielectric case ($\epsilon_{r2} = 2 + 0.01j$), for TE and TM polarizations. The parameters are the same as in Table 5 with $\theta_i = 0^\circ$ and $\sigma_z = 2\lambda_0 \Rightarrow \sigma_\gamma = \sqrt{2}$ ((a) and (c) cases). Now, the RRE is computed over the scattering coefficient, by using Equation (17) and by substituting $\mathbf{X}$ by σ_s (scattering coefficient of the FB) and $\mathbf{X}_{\mathrm{LU}}$ by $\sigma_{s,\mathrm{LU}}$ (scattering coefficient from the direct LU inversion). In the legend, the RRE is given in a linear scale. As the order P_{FB} increases, the RRE decreases and we can observe that the results converge toward the ones obtained from a direct LU inversion. The last order is given from Table 5.

Like the PILE method, Déchamps et al. [23] have recently shown that the Forward–Backward method converges if the norm (the modulus of its eigenvalue which has the highest modulus) of the characteristic matrix $\bar{\mathbf{M}}_{\mathrm{FB}}$ is smaller than one. The norm of $\bar{\mathbf{M}}_{\mathrm{FB}}$ (norm ($\bar{\mathbf{M}}_{\mathrm{FB}}$)) is a relevant criterion to study the validity of FB because it is independent of the incidence and scattering angles. It depends only on the surface profile and the permittivity ϵ_{r2}. For a single dielectric rough surface, Iodice [28] has studied in detail the convergence of the FB against the choice of the Height Autocorrelation Function (HAF). For a Gaussian HAF, the FB always converges, whereas for an exponential HAF with the same correlation length and RMS height as the Gaussian case, the FB may fail for very rough surfaces. For example, with $N_- = 800$, $L_- = 80\lambda_0$, $L_c = 2\lambda_0$, $\sigma_z = \lambda_0$, $\epsilon_{r2} = 2 + 0.01j$, $g = L_-/6$, $(\bar{\mathbf{M}}_{\mathrm{FB}}) = 0.4114 < 1$ for a Gaussian HAF, whereas (norm $\bar{\mathbf{M}}_{\mathrm{FB}}) = 2.7662 > 1$ for an exponential HAF, which means that the FB method does not converge. This is verified if we compute the scattering coefficient for different incidence and scattering angles.

4.2. *FB-SA (Spectral Acceleration) method*

First, interactions between surface points are split into strong and weak interactions. Therefore a parameter x_{d0} is introduced and defined as the horizontal distance separating the weak interactions from the strong. In the iterative procedure of the FB method, and for both forward and backward components, the strong interactions are computed exactly, whereas the weak interactions are computed approximately by using a Spectral Acceleration. The SA is based on a decomposition of the Green's function (the Weyl representation), for which the contour of integration is deformed into a steepest descent path going through the saddle point. Then, the integral in the Weyl representation can be approximated by a sum over a limited number of complex angles with an integrand modulus decaying rapidly away from the origin and a slight variation of its phase. As a result, the computation is performed only once for each surface point in the iteration since, with the appropriate contour deformation, contributions from large numbers of surface points to a single point are evaluated simultaneously. Consequently, the complexity of the FB-SA is $\mathcal{O}(N_-)$. More details can be found in [17, 18, 21, 23, 29].

As a rule of thumb x_{d0} is chosen equal to αL_c where α equals 2 or 3. A detailed study about the optimal choice for this parameter (and also the parameters which define the new integration contour) can be found in [18]. With an order P_{FB} chosen in such manner that the FB satisfies the RRE criterion given before, x_{d0} is chosen equal to $3L_c$ in order to test the convergence of the FB-SA method. In Figures 6 and 7 the field $|\psi_-|$ and its normal derivative $|\partial\psi_-/\partial n_-|$ on the surface computed from FB-SA are compared with the ones obtained from a direct LU inversion versus the normalized abscissa x/λ_0. At the top, TE case and at the bottom, TM case. PC rough surface in Figure 6, and dielectric rough surface in Figure 7. The parameters are the same as in Figure 5 and the order P_{FB} is given from Table 5. The distance of the strong interactions is $x_{d0} = 3L_c = 6\lambda_0$. We observe very good agreement. From the parameters of Table 5, similar simulations with $x_{d0} = 3L_c$ not reported in this paper, also showed very good agreement. In conclusion, in what follows x_{d0} will be equal to $3L_c$ for the spectral acceleration.

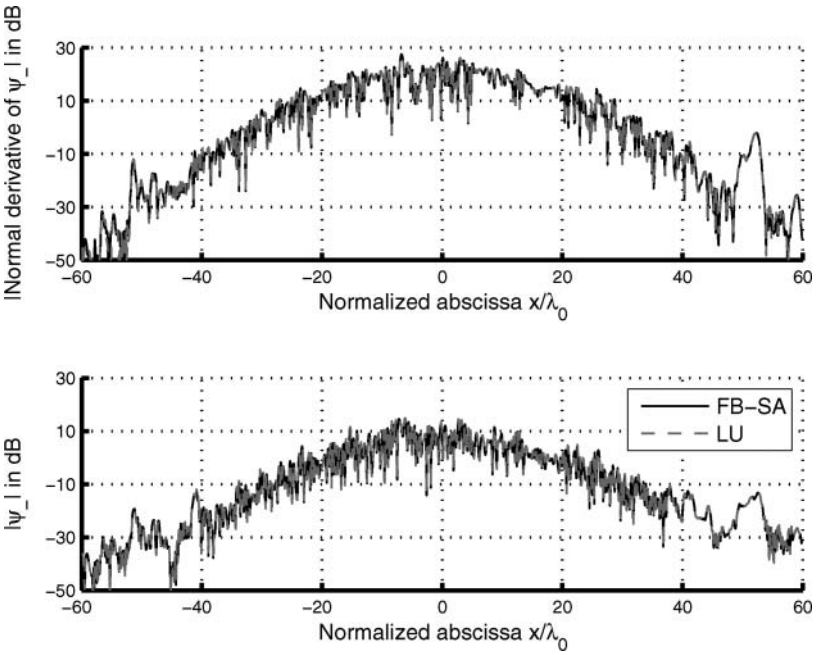

Figure 6. Comparison of the field $|\psi_-|$ and its normal derivative $|\partial\psi_-/\partial n_-|$ (without object) on the PC surface computed from FB-SA with the ones obtained from a direct LU inversion versus the normalized abscissa x/λ_0. At the top, TE case and at the bottom, TM case. The parameters are the same as in Figure 5 with $x_{d0} = 3L_c$ and the order P_{FB} is given from Table 5.

We can notice that the convergence of FB-SA seems to be not so good for the dielectric rough surface. In fact, the deformation of the integration contour obtained from the literature was evaluated only for the PC rough surface case. These slight differences show that for dielectric case, the integration contour should be deformed differently. To our knowledge, no article has been published for the SA for the single-interface dielectric case. This paper is not devoted to the extension of the integration contour calculation of the SA to dielectric surface. We will see in more detail the consequences on the results in Subsection 4.4.

4.3. *Complexity and memory space for extended PILE + FB-SA*

The number of multiplications involved in the FB-SA depends on the parameter Q which is related to the number of complex angles used for the decomposition of the Green's function. In the general case, $Q = 20$, which means for the weak interactions that the Green's function can be represented as a superposition of $2Q + 1 = 41$ plane waves.

For the complexity calculation, both the lower (the rough surface) and upper (the object) surfaces are dielectric. One can show that for an iteration number P_{FB} of the FB, the backward and forward steps applied on the four submatrices lead to $(3 + 4)(2Q + 1)(N_- - N_s) \times 2 \times 2P_{\mathrm{FB}}$ multiplications for the weak interactions, and $4N_-N_s$ for the strong interactions (N_s is the integer part of $x_{do}/\Delta x_-$). A direct LU inversion of $\bar{\mathbf{Z}}_+$ leads to $N_+^3/3$ multiplications. So the computation of the characteristic matrix requires $8N_+N_- + 2N_+2N_+$ for the matrix-vector products, and $N_+^3/3 + [28(2Q + 1)(N_- - N_s) + 4N_-N_s]\, P_{\mathrm{FB}}$ for the inversions.

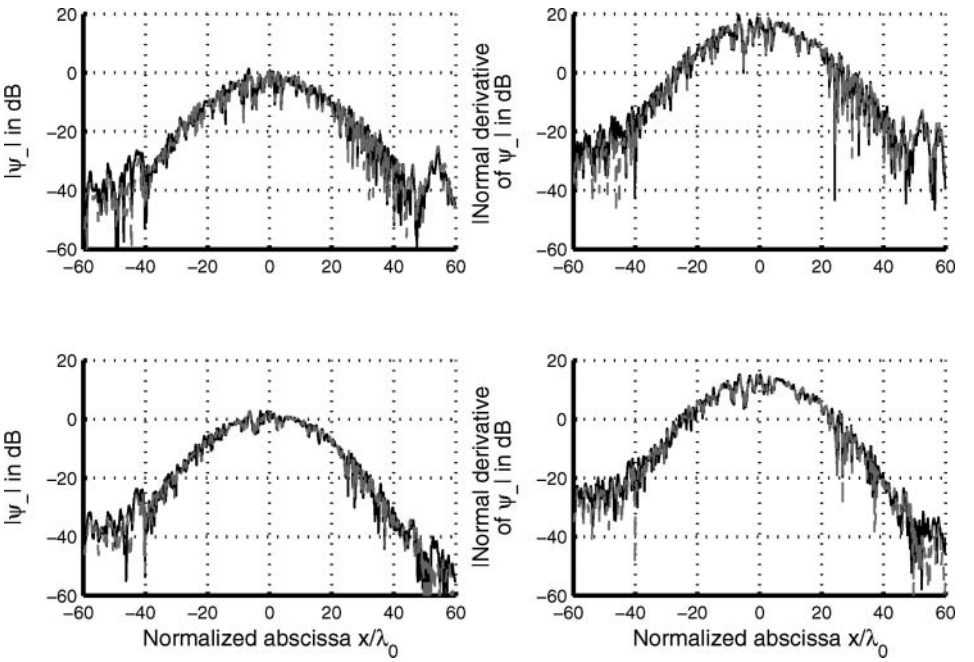

Figure 7. Comparison of the field $|\psi_-|$ and its normal derivative $|\partial\psi_-/\partial n_-|$ (without object) on the dielectric surface computed from FB-SA with the ones obtained from a direct LU inversion versus the normalized abscissa x/λ_0. At the top, TE case and at the bottom, TM case. The parameters are the same as in Figure 5 with $x_{d0} = 3L_c$ and the order P_{FB} is given from Table 5.

In conclusion, from Equation (15), the computation of $\mathbf{X}_+$ and $\mathbf{X}_-$ at the order P_{PILE} with extended PILE combined with FB-SA needs

$$
\begin{aligned}
&2\Big\{8N_+N_- + 4N_+^2 \text{ (matrix-vector products)}\\
&\quad + \big[28(2Q+1)(N_- - N_s) + 4N_-N_s\big]P_{\mathrm{FB}} \text{ (inversion of } \bar{\mathbf{Z}}_-)\Big\}P_{\mathrm{PILE}}\\
&\quad + 2\Big\{\big[28(2Q+1)(N_- - N_s) + 4N_-N_s\big]P_{\mathrm{FB}} + 4N_+N_- + 4N_+^2\Big\}\\
&\quad \text{(order 0, inversion of } \bar{\mathbf{Z}}_- \text{ and matrix-vector products)}\\
&\quad + 8N_+^3/3 \text{ (initialization: inversion of } \bar{\mathbf{Z}}_+)
\end{aligned}
\tag{22}
$$

operations, instead of $8N_+^3/3 + 8N_-^3/3 + 2(4N_+^2 + 4N_-^2 + 4N_+N_-) + 2(8N_+N_- + 4N_+^2 + 4N_-^2)P_{\mathrm{PILE}}$ from PILE. At order 0, since $N_- \gg N_s$ and $N_- \gg 1$, PILE+FB-SA is fast compared to PILE if $8N_-^2/3 \gg [28(2Q+1) + 4N_s]\,P_{\mathrm{FB}}$. Typically, $N_s = 100$, $P_{\mathrm{FB}} = 5$, $Q = 20$, thus $N_- \gg 54$. At the order P_{PILE}, we must have $4N_- \gg [28(2Q+1) + 4N_s]\,P_{\mathrm{FB}}$, which leads to $N_- \gg 1935$. But, the storage of the inverse of $\bar{\mathbf{Z}}_-$ is not necessary unlike PILE. Indeed with FB-SA, only the submatrix elements of $\bar{\mathbf{Z}}_-$ of the strong interactions must be stored. For a submatrix, the number of elements is $N_s(N_s+1)/2 + (N_- - N_s - 1)N_s$, which leads to N_-N_s for $N_- \gg N_s$ instead of N_-^2.

In order to obtain the complexity and the memory space for PILE+FB-SA with a PC elliptic cylinder and/or a PC rough surface, the number of unknowns N_+ and/or N_- must be divided by 2.

4.4. *Numerical results*

In this section, the extended PILE method combined with FB-SA and referred to as PILE+FB-SA is compared with the results obtained from a direct LU inversion of the impedance matrix $\bar{\mathbf{Z}}$. The input parameter of PILE is its order P_{PILE} (see Equation 15), which is related to the number of reflections between the object and the rough surface. The order P_{FB} of the FB method for the inversion of the impedance matrix of the rough surface is an input parameter, with the order P_{PILE}, of PILE+FB. For PILE+FB-SA, the input parameters are P_{PILE}, P_{FB} and x_{d0}, which is the distance of the strong interactions required for the calculation of the integration contour. First, the convergence of PILE+FB-SA is investigated. Finally, the computation time of PILE+FB-SA is presented.

4.4.1. *Convergence of PILE+FB-SA*

The parameters of the FB-SA, needed to calculate the local interactions on the rough surface, are given in Table 5. In addition, the distance of the strong interactions is $x_{d0} = 3L_c$.

In Figure 8, for the TE case, the modulus of the field ψ_+ on the rough surface is plotted versus the normalized abscissa x/λ_0: the PC rough surface case ($\epsilon_{r2} = j\infty$) in Figure 8(a) and the dielectric rough surface case ($\epsilon_{r2} = 2 + 0.01j$) in Figure 8(b). The parameters are $\theta_i = 0^\circ$, $L_c = 2\lambda_0$, $\sigma_z = \lambda_0$, sampling step $\lambda_0/10$ ($N_- = 1200$) for the rough surface of length $L_- = 120\lambda_0$, $g = L_-/6$, $N_+ = 63$, $h_c = 4\lambda_0$ and $a = 1\lambda_0$. Top, PILE method. Middle, PILE+FB method with P_{FB} obtained from Table 5 (6 for the PC surface and 5 for the dielectric one). Bottom, PILE+FB-SA method with $x_{d0} = 3L_c$. In each subfigure, the order of PILE and the corresponding RRE are mentioned in the legend. In addition, the results computed from a direct LU inversion are plotted. At the top, we can observe that the PILE method converges after three iterations in PC case and only 1 iteration for the dielectric case, which means that the number of back and forth between the object and the surface in medium Ω_1 contributing to the scattering process is $P_{\text{PILE}} = 3$ for the PC case. In addition, Figure 8 reveals that the field vanishes on the surface edges. As seen in Subsection 3.2, this condition must be satisfied to apply the integral equations. Moreover, Figure 8 shows also that the PILE method combined with FB presents good convergence, which means that the order P_{FB} is well chosen. One can see that there is no differences between the PILE+FB method and PILE+FB-SA for the PC surface case. So, the SA is well used in this approach. Nevertheless, for the dielectric surface case, the PILE+FB-SA approach is not perfect. Although the observation of the curve seems to indicate good convergence, the RRE remains constant after the PILE method converged. Indeed, the SA in the dielectric case does not converge at the order 0 when the local interactions are calculated on the rough surface. As seen before in Subsection 4.2, the integration contour of the SA, for dielectric case, should be deformed differently. But, as displayed in Figure 9, the impact on the scattering coefficient is minor except for grazing scattering angles. Now, the RRE is computed over the scattering coefficient, by using Equation (17) and by substituting $\mathbf{X}$ by σ_s (scattering coefficient) and $\mathbf{X}_{\text{LU}}$ by $\sigma_{s,\text{LU}}$ (scattering coefficient from the direct LU inversion). In the legend, the RRE is given in a linear scale.

Figures 10(a) and 10(b) compare the RRE over the scattering coefficient versus the normalized RMS height σ_z/λ_0 for the TE and TM polarizations, respectively. The orders P_{FB} and P_{PILE} are obtained from Tables 1 and 5, in which the (a) case is considered (PC rough surface). As we can see, the RRE is of the order of 10^{-2} for PILE, whereas it is slightly higher for FB and FB-SA.

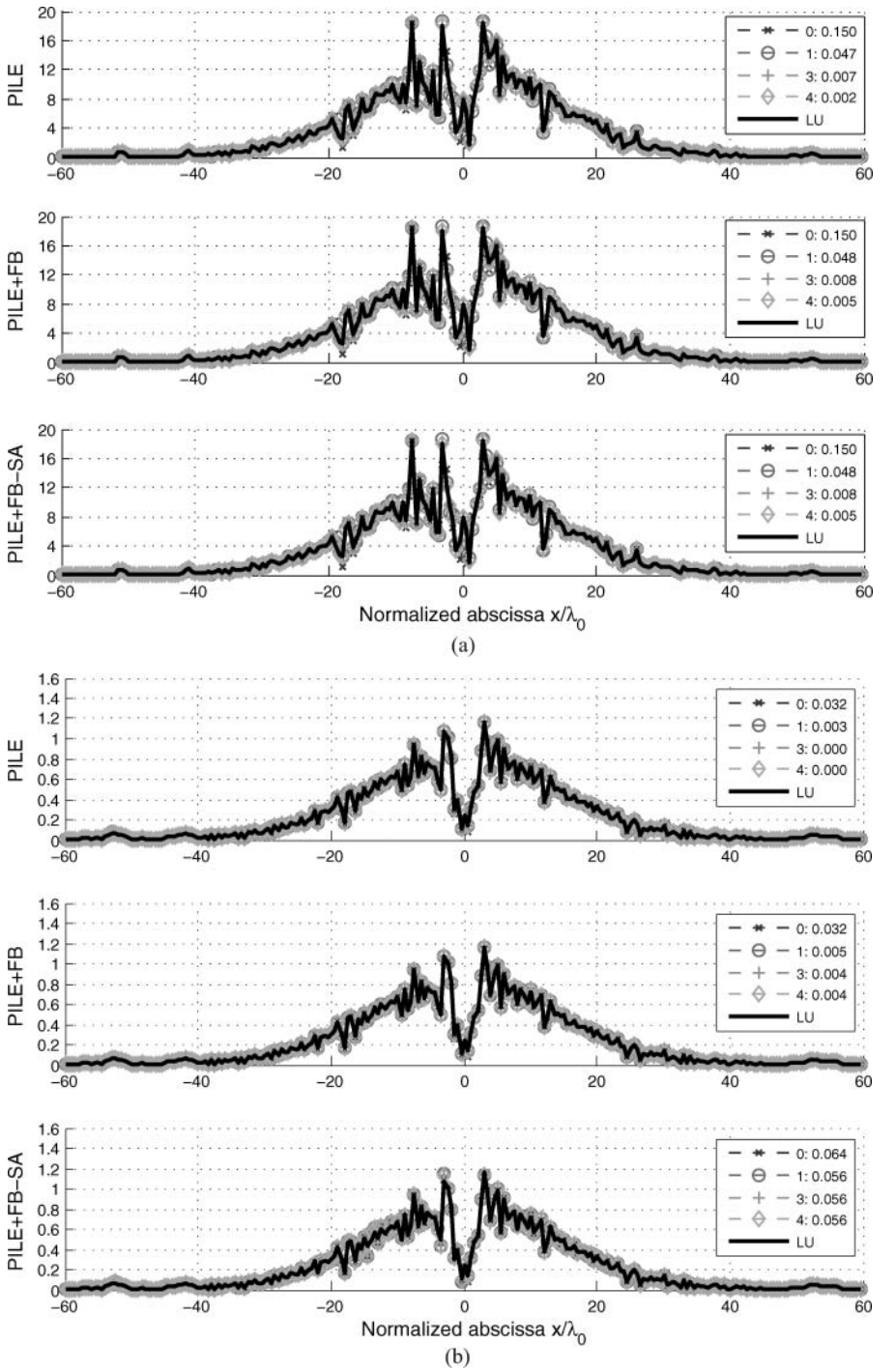

Figure 8. Modulus $|\psi_-|$ on the rough surface versus the normalized abscissa x/λ_0 for the TE case. $\theta_i = 0^\circ$, $L_c = 2\lambda_0$, $\sigma_z = \lambda_0$, $N_- = 1200$, $L_- = 120\lambda_0$, $g = L_-/6$, $N_+ = 63$, $h_c = 4\lambda_0$ and $a = 1\lambda_0$. Top, PILE method. Middle, PILE+FB method with P_{FB} chosen from Table 5. Bottom, PILE+FB-SA method with $x_{d0} = 3L_c$. In each subfigure, the order of PILE and the corresponding RRE are mentioned in the legend. In addition, the results computed from a direct LU inversion are plotted. At the top, PC rough surface case ($\epsilon_{r2} = j\infty$), and at the bottom dielectric rough surface case ($\epsilon_{r2} = 2 + 0.01j$).

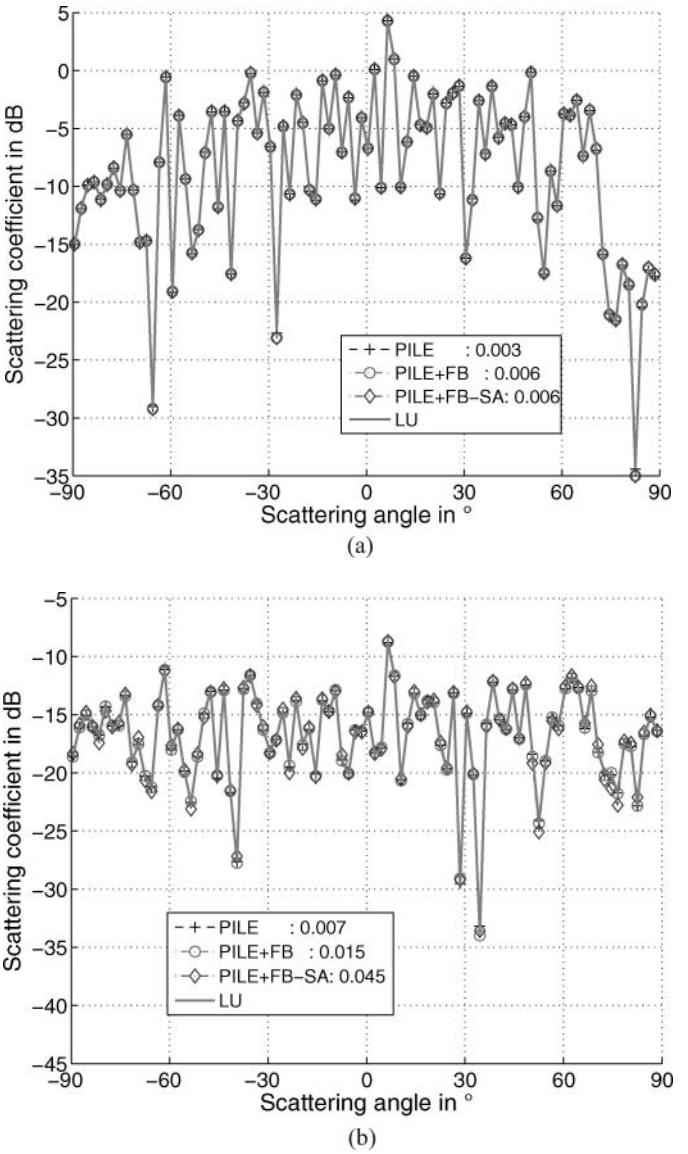

Figure 9. Comparison of the scattering coefficient in the dB scale with the one obtained from a direct LU inversion versus the scattering angle θ_s. In addition the RRE computed over the scattering coefficient are given. The parameters are the same as in Figure 8. At the top, PC rough surface case ($\epsilon_{r2} = j\infty$), and at the bottom dielectric rough surface case ($\epsilon_{r2} = 2 + 0.01j$).

The RRE for the FB and the FB-SA are equal, which shows the good convergence of the SA. In the same manner, Figures 11(a) and 11(b) compare the RRE over the scattering coefficient versus the normalized RMS height σ_z/λ_0 for the TE and TM polarizations, respectively. The orders P_{FB} and P_{PILE} are obtained from Tables 5 and 1, in which the (c) case is considered (dielectric rough surface). As we can see, the RRE is of the order of 10^{-2} for PILE, whereas it is proportional to the RMS height for FB and FB-SA and it is few sensible to the polarization. In addition, the RRE is larger for FB-SA.

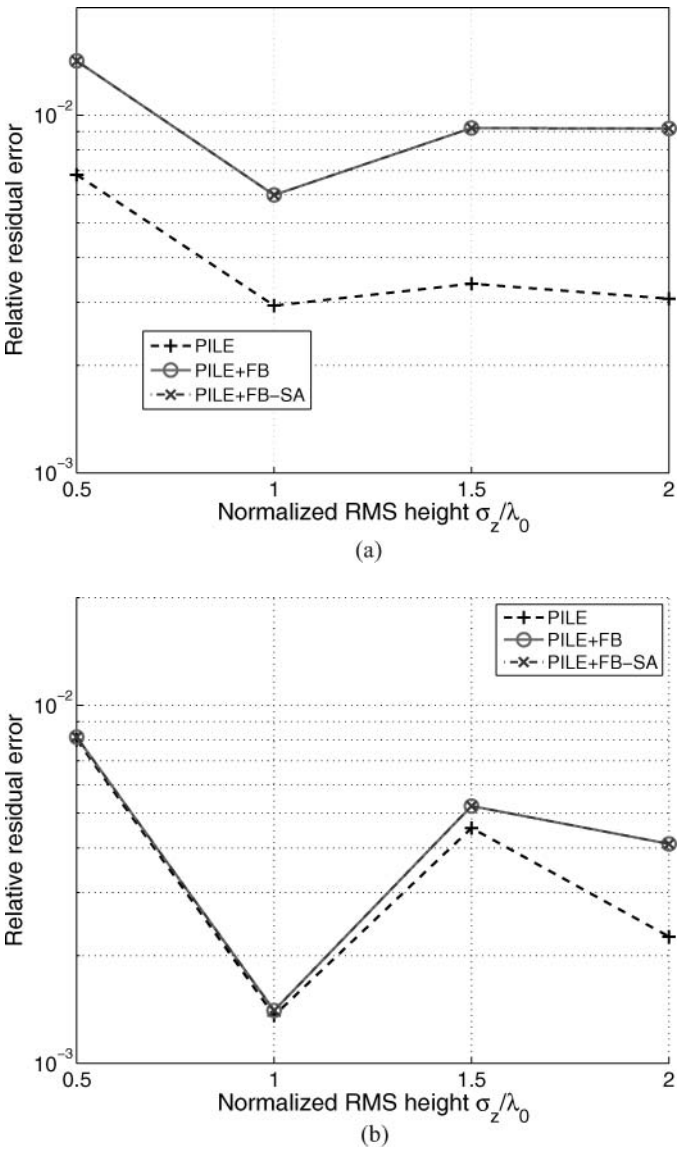

Figure 10. Comparison of the RRE over the scattering coefficient versus the normalized RMS height σ_z/λ_0. The orders P_{FB} and P_{PILE} are obtained from Tables 5 and 1, in which the (a) case is considered (PC rough surface). At the top, TE polarization and at the bottom, TM polarization.

In order to see how the FB-SA converges to the FB according to the distance x_{d0}, in Figure 12 the RRE over the scattering coefficient is plotted versus x_{d0}/L_c for the TE and TM polarizations. The parameters are the same as in Figure 8(b) and the orders $\{P_{\mathrm{FB}} = 5,\ P_{\mathrm{PILE}} = 1\}$ for the TE and TM polarizations. We can observe that the RRE decreases slowly with x_{d0} and reaches the value obtained from PILE+FB for $x_{d0} \geq 40L_c$. As expected, the same study for a PC rough surface case, not presented here, shows very good convergence of the FB-SA from $x_{d0} \geq 3L_c$.

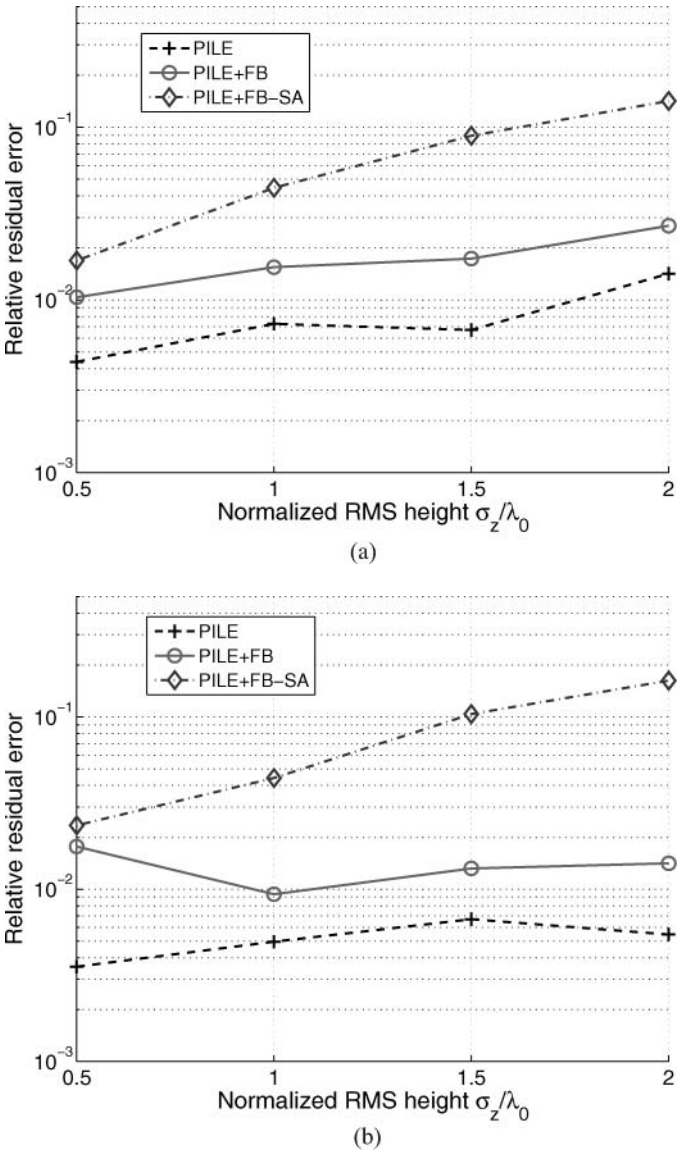

Figure 11. Same variations as in Figure 10 but for a dielectric surface ((c) case in Table 1) (a) TE case (b) TM case.

4.4.2. *Computation time of PILE + FB-SA*

In Figure 13 the CPU time t_{CPU} of the PILE+FB−SA is plotted versus the number of samples N_- on the rough surface. The parameters are the same as in Figure 8(a) but $\sigma_z = 0.5\lambda_0$, with $\{P_{\mathrm{FB}} = 5,\ P_{\mathrm{PILE}} = 2\}$ and $\{P_{\mathrm{FB}} = 1,\ P_{\mathrm{PILE}} = 2\}$ for the TE and TM polarizations (Tables 5 and 1), respectively. It should be noted that the number of unknowns are $N_- + N_+ = N_- + 63$. In addition, results obtained from a linear regression (TE case: $t_{\mathrm{CPU}} = -155.8847 + 0.00490N_-$; TM case: $t_{\mathrm{CPU}} = -30.1158 + 0.00096N_-$) are displayed. A 3.4 GHz personal computer with

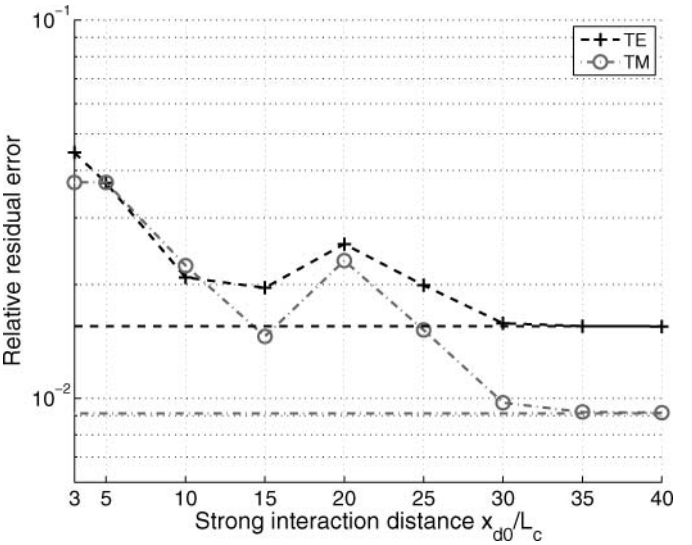

Figure 12. RRE over the scattering coefficient of PILE+FB-SA versus the normalized distance x_{d0}/L_c for the TE and TM polarizations. The parameters are the same as in Figure 8(b). The horizontal lines indicate the values of RRE of PILE+FB obtained from Figures 11(a) and 11(b) with $\sigma_z = \lambda_0$.

2 GB of RAM with the MATLAB software is used in this work. We can observe that the CPU time of PILE+FB-SA is approximately proportional to N_-. Nevertheless, the CPU time for the TE polarization is larger because the product $P_{\mathrm{FB}} P_{\mathrm{PILE}}$ is larger than the one obtained from the TM polarization. In fact, the ratio of the slope of the regression straight

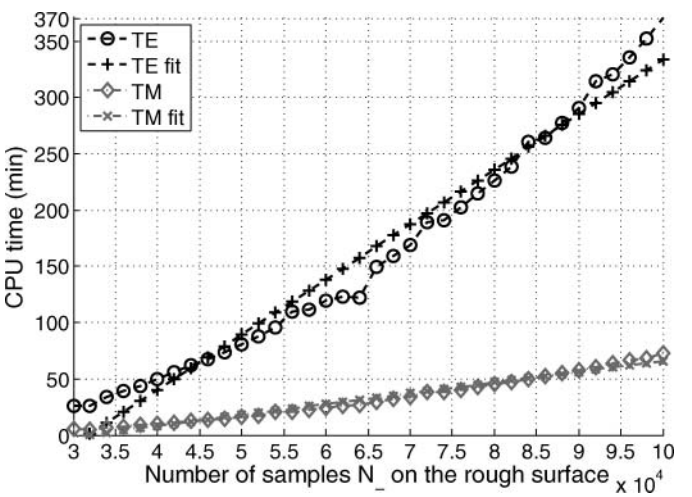

Figure 13. CPU time versus the number of samples N_- on the PC rough surface. The parameters are the same as Figure 8(a) but $\sigma_z = 0.5\lambda_0$, with $\{P_{\mathrm{FB}} = 5,\ P_{\mathrm{PILE}} = 2\}$ and $\{P_{\mathrm{FB}} = 1,\ P_{\mathrm{PILE}} = 2\}$ for the TE and TM polarizations (Tables 1 and 5), respectively. The number of unknowns is $N_- + N_+ = N_- + 63$.

line for each polarization is approximately equal to the ratio computed from $P_{\mathrm{FB}}(P_{\mathrm{PILE}}+1)$. Thus, as expected, the CPU time is of the order of $P_{\mathrm{FB}}(P_{\mathrm{PILE}}+1)\mathcal{O}(N_-)$. One of the advantages of PILE+FB-SA is to be able to treat large problem from a personal computer. For instance, for $N_- = 100,000$ and $N_+ = 63$, the number of unknowns is 100,063. In this case, the PILE+FB-SA requires to store 63^2 (for $\bar{\mathbf{Z}}_+$) $+ 2 \times 63 \times 100,000$ (coupling matrices) $+ 2 \times 9,994,950$ (strong interactions for $\bar{\mathbf{Z}}_-$) $= 32,593,869$ complex values, which corresponds to $2 \times 16 \times 32,593,869/8/1024^2 \approx 124$ Mo of memory.

5. Conclusion

In this paper, a new efficient method to predict the field scattered from a homogeneous object located above a one-dimensional dielectric rough surface has been presented. The method is based on the rigorous PILE method, originally developed for a stack of two one-dimensional rough interfaces separating homogeneous media, and extended in this work to two illuminated surfaces. This extended PILE method was applied to the case of an elliptic cylinder above a surface. In addition, for the calculation of the local interactions of the rough surface, the extended PILE method was accelerated using the fast method, Forward–Backward (FB), combined with a Spectral Acceleration (SA). The resulting method, the extended PILE+FB-SA, has then a complexity of $\mathcal{O}(N_-)$, in which N_- is the number of samples on the rough surface, if $N_- \gg N_+$ (number of the samples on the object).

The numerical results showed that the PILE method converges rapidly. Indeed, the PILE order is linked to the number of reflections between the object and the rough surface contributing to the scattering process. Combined with FB, the PILE+FB converges also rapidly for the FB step (about six iterations for $\epsilon_{r2} = j\infty$ and $\epsilon_{r2} = 2 + 0.01j$ and about 10 iterations for $\epsilon_{r2} = 10 + j$, see Table 5). One of the advantages of PILE+FB, is that the order P_{FB} of the FB step, can be obtained from the study of the scattering from a single rough surface. PILE+FB combined with SA presents good convergence for a quite rough surface with a distance of strong interactions of the order of $3L_c$ (height correlation length). As the surface roughness increases (RMS height), this distance must be increased.

Instead of using the FB-SA approach to accelerate the calculation of the local interactions on the rough surface, the Banded-Matrix-Iterative-Approach/CAnonical Grid (BMIA-CAG) developed by Tsang et al. could be applied. This method of complexity $\mathcal{O}(N_- \log N_-)$ is interesting for RMS heights approximately smaller than $3\lambda_0$. Moreover, as prospects of this paper, it could be interesting to apply the PILE+FB-SA to several objects above a rough surface and to improve the calculation of the integration contour for the SA when a dielectric rough surface is considered.

References

[1] A. Sommerfeld, *Lectures on Theoretical Physics*, Vol. 6, Academic, New York, 1964.
[2] G. Videen, *Light scattering from a sphere on or near a surface*, J. Opt. Soc. Amer. A 8 (1991), pp. 483–489.
[3] G.Videen and D. Ngo, *Light scattering from a cylinder near a plane interface: Theory and comparison with experimental data*, J. Opt. Soc. Amer. A 14 (1997), pp. 70–78.
[4] P.J. Valle, F. Gonzalez, and F. Moreno, *Electromagnetic wave scattering from conducting cylindrical structures on flat substrates: Study by means of the extinction theorem*, Appl. Opt. 33 (1994), pp. 512–523.
[5] A. Madrazo and M. Nieto-Vesperinas, *Scattering of electromagnetic waves from a cylinder in front of a conducting plane*, J. Opt. Soc. Amer. A 12 (1995), pp. 1298–1309.
[6] J.T. Johnson, *A study of the four-path model for scattering from an object above a half space*, Microwave Opt. Technol. Lett. 30 (2001), pp. 130–134.

[7] M.R. Pino, L. Landesa, J.L. Rodriguez, F. Obelleiro, and R. Burkholder, *The generalized Forward–Backward method for analyzing the scattering from targets on ocean-like rough surfaces*, IEEE Trans. Antennas Propagat. 47 (1999), pp. 961–969.

[8] J.T. Johnson, *A numerical study of scattering from an object above a rough surface*, IEEE Trans. Antennas Propagat. 50 (2002), pp. 1361–1367.

[9] X. Wang, C.-F. Wang, Y.-B. Gan, and L.-W. Li, *Electromagnetic scattering from a circular target above or below rough surface*, Prog. Electromag. Res. 40 (2003), pp. 207–227.

[10] P. Liu and Y.Q. Jin, *The Finite-Element Method with domain decomposition for electromagnetic bistatic scattering from the comprehensive model of a ship on and a target above a large scale rough sea surface*, IEEE Trans. Geosci. Remote Sens. 42 (2004), pp. 950–956.

[11] H. Ye and Y. Jin, *Fast iterative approach to difference electromagnetic scattering from the target above a rough surface*, IEEE Trans. Geosci. Remote Sens. 44 (2006), pp. 108–115.

[12] C. Dong, C. Wang, X. Wei, and H.Yin, *EM scattering from complex targets above a slightly rough surface*, PIERS Online 3 (2007), pp. 685–688.

[13] H. Ye and Y.-Q. Jin, *A hybrid analytic-numerical algorithm of scattering from an object above a rough surface*, IEEE Trans. Antennas Propagat. 45 (2007), pp. 1174–1180.

[14] L. Tsang, C.H. Chang, and H. Sangani, *A Banded Matrix Iterative Approach to Monte Carlo simulations of scattering of waves by large scale random rough surface problems: TM case*, Electron. Lett. 29 (1993), pp. 1666–1667.

[15] L. Tsang, C.H. Chang, H. Sangani, A. Ishimaru, and P. Phu, *A Banded Matrix Iterative Approach to Monte Carlo simulations of large scale random rough surface scattering: TE case*, J. Electromag. Waves Appl. 29 (1993), pp. 1185–1200.

[16] D. Holliday, L.L. DeRaad Jr., and G.J. St-Cyr, *Forward–Backward: A new method for computing low-grazing angle scattering*, IEEE Trans. Antennas Propagat. 44 (1995), pp. 1199–1206.

[17] H.T. Chou and J.T. Johnson, *A novel acceleration algorithm for the computation of scattering from rough surfaces with the Forward–Backward method*, Radio Sci. 33 (1998), pp. 1277–1287.

[18] D. Torrungrueng, J.T. Johnson, and H.T. Chou, *Some issues related to the Novel Spectral Acceleration method for the fast computation of radiation/scattering from one-dimensional extremely large scale quasi-planar structures*, Radio Sci. 37 (2002), pp. 1–20.

[19] M.R. Pino, R. Burkholder, and F. Obelleiro, *Spectral acceleration of the generalized Forward–Backward method*, IEEE Trans. Antennas Propagat. 50 (2002), pp. 785–797.

[20] N. Déchamps, N. De Beaucoudrey, C. Bourlier, and S. Toutain, *Fast numerical method for electromagnetic scattering by rough layered interfaces: Propagation-Inside-Layer Expansion method*, J. Opt. Soc. Amer. A. 23 (2006), pp. 359–369.

[21] C. Bourlier, G. Kubické, and N. Déchamps, *A fast method to compute scattering by a buried object under a randomly rough surface: PILE combined to FB-SA*, J. Opt. Soc. Amer. A 25 (2008), pp. 891–902.

[22] N. Déchamps and C. Bourlier, *Electromagnetic scattering from a rough layer: Propagation-Inside-Layer Expansion method combined to an updated BMIA/CAG approach*, IEEE Trans. Antennas Propagat. 55 (2007), pp. 2790–2802.

[23] N. Déchamps and C. Bourlier, *Electromagnetic scattering from a rough layer: Propagation-Inside-Layer Expansion method combined to the Forward–Backward Novel Spectral Acceleration*, IEEE Trans. Antennas Propagat. 55 (2007), pp. 3576–3586.

[24] L. Tsang, J.A. Kong, K.-H. Ding, and C.O. Ao, *Scattering of Electromagnetics Waves: Numerical Simulations*, John Wiley, New York, 2001.

[25] E.I. Thorsos, *The validity of the Kirchhoff approximation for rough surface scattering using a Gaussian roughness spectrum*, J. Opt. Soc. Amer. 83 (1988), pp. 78–92.

[26] A. Madrazo and M. Nieto-Vesperinas, *Scattering of light and other electromagnetic waves from a body buried beneath a highly rough random surface*, J. Opt. Soc. Amer. 14 (1997), pp. 1859–1866.

[27] W.H. Press, S.A. Teutolsky, W.T. Vetterling, and B.P. Flannery, *Numerical Recipies*, 2nd edn, Cambridge University Press, Cambridge, 1992.

[28] A. Iodice, *Forward–Backward method for scattering from dielectric rough surfaces*, IEEE Trans. Antennas Propagat., 50 (2002), pp. 901–911.

[29] H. T. Chou and J.T. Johnson, *Formulation of Forward–Backward method using Novel Spectral Acceleration for the modeling of scattering from impedance rough surfaces*, IEEE Trans. Geosci. Remote Sens. 38 (2000), pp. 605–607.

Appendix A: Submatrix expressions of the impedance matrix

For a dielectric object located above a dielectric surface, the submatrices $\{\bar{\mathbf{Z}}_+, \bar{\mathbf{Z}}_-, \bar{\mathbf{Z}}_\pm, \bar{\mathbf{Z}}_\pm\}$ are expressed from elementary submatrices as

$$\bar{\mathbf{Z}}_+ = \begin{bmatrix} \bar{\mathbf{A}}_+ & \bar{\mathbf{B}}_+ \\ \bar{\mathbf{C}}_+ & \rho_{31}\bar{\mathbf{D}}_+ \end{bmatrix} \quad \bar{\mathbf{Z}}_- = \begin{bmatrix} \bar{\mathbf{A}}_- & \bar{\mathbf{B}}_- \\ \bar{\mathbf{C}}_- & \rho_{21}\bar{\mathbf{D}}_- \end{bmatrix}, \tag{A1}$$

and

$$\bar{\mathbf{Z}}_\pm = \begin{bmatrix} \bar{\mathbf{A}}_\pm & \bar{\mathbf{B}}_\pm \\ \bar{\mathbf{0}} & \bar{\mathbf{0}} \end{bmatrix} \quad \bar{\mathbf{Z}}_\mp = \begin{bmatrix} \bar{\mathbf{A}}_\mp & \bar{\mathbf{B}}_\mp \\ \bar{\mathbf{0}} & \bar{\mathbf{0}} \end{bmatrix} \tag{A2}$$

in which $\{\rho_{31} = \epsilon_{r3}/\epsilon_{r1}, \rho_{21} = \epsilon_{r2}/\epsilon_{r1}\}$ for TM polarization, and $\{\rho_{31} = \rho_{21} = 1\}$ for TE polarization.

The elementary square matrix $\bar{\mathbf{A}}_-$ (size $N_- \times N_-$) corresponds to the matrix of a perfectly conducting surface for TM polarization (Neumann boundary condition). The elements are given by

$$A_-^{m,n} = \begin{cases} -\dfrac{jK_1\Delta x_-}{4}\dfrac{H_1^{(1)}\left(K_1\|\mathbf{r}_-^n - \mathbf{r}_-^m\|\right)}{\|\mathbf{r}_-^n - \mathbf{r}_m^-\|}[\gamma_-^n(x_-^n - x_-^m) - (z_-^n - z_-^m)] & \text{for } m \neq n \\ +\dfrac{1}{2} - \dfrac{\Delta x_-}{4\pi}\dfrac{(\gamma_-^m)'}{1+(\gamma_-^m)^2} & \text{for } m = n \end{cases}, \tag{A3}$$

with $\gamma_- = \partial z_-/\partial x_-$, $(\gamma_-)' = \partial\gamma_-/\partial x_-$, and $H_1^{(1)}$ the Hankel function of first order and first kind. $K_1 = K_0\sqrt{\epsilon_{r1}}$ is the wavenumber in the incident medium Ω_1, and K_0 stands for the wavenumber in the vacuum.

The elementary square matrix $\bar{\mathbf{B}}_-$ (size $N_- \times N_-$) corresponds to the matrix of a perfectly conducting surface for TE polarization (Dirichlet boundary condition). The elements are given by

$$B_-^{m,n} = \frac{j\Delta x_-\alpha_-^n}{4}\begin{cases} 1 + \frac{2j}{\pi}\ln(0.164K_1\alpha_-^m\Delta x_-) & \text{for} \quad n = m \\ H_0^{(1)}(K_1\|\mathbf{r}_-^n - \mathbf{r}_-^m\|) & \text{for} \quad n \neq m \end{cases}, \tag{A4}$$

with $\alpha_-^n = [1 + (\gamma_-^n)^2]^{1/2}$. The elementary matrices $\{\bar{\mathbf{C}}_-, \bar{\mathbf{D}}_-\}$ are obtained from $\{\bar{\mathbf{A}}_-, \bar{\mathbf{B}}_-\}$ by substituting in Equations (A3) and (A4), K_1 for K_2. In addition, the diagonal elements of $\bar{\mathbf{C}}_-$ equal $-\frac{1}{2} - \frac{\Delta x_-}{4\pi}\frac{(\gamma_-^m)'}{1+(\gamma_-^m)^2}$.

The elementary matrices of the object $\{\bar{\mathbf{A}}_+, \bar{\mathbf{B}}_+, \bar{\mathbf{C}}_+, \bar{\mathbf{D}}_+\}$ of size $N_+ \times N_+$ are obtained from $\{\bar{\mathbf{A}}_-, \bar{\mathbf{B}}_-, \bar{\mathbf{C}}_-, \bar{\mathbf{D}}_-\}$ by substituting in Equations (A3) and (A4), $(K_2, \text{subscript} -)$ for $(K_3, \text{subscript} +)$, respectively. For an elliptic cylinder of parametric equations $\{x_+ = x_c + a\cos\phi, z_+ = h_c + b\sin\phi\}$, $\gamma_+^n = -\frac{b}{a}\cot\phi$. Moreover, in (A3), the normal of the object must be oriented toward the external of the object, so Δx_+ is replaced by $v\,|\Delta x_+|$ in which $v = +1$ for $\phi \in [0;\pi]$, $v = -1$ otherwise. Like for the lower surface, the surface elements must be always positive. So, $v\Delta x_+$ is replaced by $v\,|\Delta x_+| = -\Delta x_+ = +a\sin\phi\Delta\phi$. In the same manner and for same reasons, in (A4), we must take the absolute values on $|\alpha_+^n\Delta x_+| = \sqrt{a^2\sin^2\phi + b^2\cos^2\phi}\,|\Delta\phi|$.

The coupling matrix $\bar{\mathbf{A}}_\mp$ (size $N_- \times N_+$) is similar to $\bar{\mathbf{A}}_-$ and its elements are expressed as

$$A_\mp^{m,n} = -\frac{jK_1\Delta x_-}{4}\frac{H_1^{(1)}(K_1\|\mathbf{r}_-^n - \mathbf{r}_+^m\|)}{\|\mathbf{r}_-^n - \mathbf{r}_+^m\|}[\gamma_-^n(x_-^n - x_+^m) - (z_-^n - z_+^m)]. \tag{A5}$$

The coupling matrix $\bar{\mathbf{B}}_\mp$ (size $N_- \times N_+$) is similar to $\bar{\mathbf{B}}_-$ and its elements are expressed as

$$B_\mp^{m,n} = +\frac{j\alpha_-^n\Delta x_-}{4}H_0^{(1)}(K_1\|\mathbf{r}_-^n - \mathbf{r}_+^m\|). \tag{A6}$$

The elementary matrices $\{\bar{\mathbf{A}}_{\pm}, \bar{\mathbf{B}}_{\pm}\}$ of size $N_+ \times N_-$ are obtained from $\{\bar{\mathbf{A}}_{\mp}, \bar{\mathbf{B}}_{\mp}\}$ by substituting in Equations (A5) and (A6) the subscripts $(+, -)$ for the subscripts $(-, +)$, respectively. Moreover, and like for the matrices $\{\bar{\mathbf{A}}_+, \bar{\mathbf{B}}_+, \bar{\mathbf{C}}_+, \bar{\mathbf{D}}_+\}$, Δx_+ is replaced by $-\Delta x_+$ in Equation (A5), and $\alpha_+^n \Delta x_+$ is replaced by $|\alpha_+^n \Delta x_+|$ in Equation (A6).

If the object is assumed to be a perfect conductor whereas the rough surface is dielectric, then $\bar{\mathbf{Z}}_{\mp} = [\bar{\mathbf{A}}_{\mp}\ \bar{\mathbf{B}}_{\mp}]$. Moreover, the submatrices $\{\bar{\mathbf{Z}}_+, \bar{\mathbf{Z}}_{\pm}\}$ and the unknown vector $\mathbf{X}_+$ become

$$\begin{cases} \text{TE case: } \bar{\mathbf{Z}}_+ = \bar{\mathbf{B}}_+ \ \bar{\mathbf{Z}}_{\pm} = \begin{bmatrix} \bar{\mathbf{B}}_{\pm} \\ \bar{0} \end{bmatrix} \mathbf{X}_+ \equiv \dfrac{\partial \psi_+}{\partial n_+} \\ \text{TM case: } \bar{\mathbf{Z}}_+ = \bar{\mathbf{A}}_+ \ \bar{\mathbf{Z}}_{\pm} = \begin{bmatrix} \bar{\mathbf{A}}_{\pm} \\ \bar{0} \end{bmatrix} \mathbf{X}_+ \equiv \psi_+ \end{cases} . \tag{A7}$$

If the object and the rough surface are assumed to be perfect conductors, then the submatrices $\{\bar{\mathbf{Z}}_+, \bar{\mathbf{Z}}_{\pm}, \bar{\mathbf{Z}}_-, \bar{\mathbf{Z}}_{\pm}\}$ and the unknown vectors $\mathbf{X}_+$ and $\mathbf{X}_-$ become

$$\begin{cases} \text{TE case:} \bar{\mathbf{Z}}_+ = \bar{\mathbf{B}}_+ \ \ \bar{\mathbf{Z}}_{\pm} = \bar{\mathbf{B}}_{\pm} \ \bar{\mathbf{Z}}_- = \bar{\mathbf{B}}_- \ \bar{\mathbf{Z}}_{\mp} = \bar{\mathbf{B}}_{\mp} \ \mathbf{X}_+ \equiv \dfrac{\partial \psi_+}{\partial n_+} \ \mathbf{X}_- \equiv \dfrac{\partial \psi}{\partial n_-} \\ \text{TM case:} \bar{\mathbf{Z}}_+ = \bar{\mathbf{A}}_+ \ \bar{\mathbf{Z}}_{\pm} = \bar{\mathbf{A}}_{\pm} \ \bar{\mathbf{Z}}_- = \bar{\mathbf{A}}_- \ \bar{\mathbf{Z}}_{\mp} = \bar{\mathbf{A}}_{\mp} \ \mathbf{X}_+ \equiv \psi_+ \quad \mathbf{X}_- \equiv \psi_- \end{cases} . \tag{A8}$$